Generalized analytical solution for compressive forces in adhesively-bonded-joint assembling

L. Bergamasco, S. Izquierdo*, E. Duvivier, J.M. Royo, A. Chiminelli, M.A. Jiménez

Instituto Tecnológico de Aragón (ITA) - María de Luna 8, 50018 Zaragoza, Spain

Abstract

Normal forces exerted by the adhesive to the substrate during the squeeze flow occurring in compaction of bonded joints are analyzed using theoretical, numerical and experimental techniques. An analytical solution, derived from the squeeze-flow theory of a viscoplastic material, is generalized to be valid for any initial shape of the adhesive cord. The rheology of the material is modeled according to the Herschel-Bulkley model and is fitted with experimental data available from the characterization of an epoxy-based adhesive. The analytical law is compared with a numerical model, where the two-phase problem for the squeeze-flow test is solved by finite-volume methods using a commercial CFD solver. The results obtained with these two approaches show excellent agreement with experimental forces obtained for a wedge-shaped specimen. The proposed methodology can therefore be useful for the optimization of the bond lines in assembling processes.

Keywords: Squeeze forces, adhesively-bonded joints, Herschel-Bulkley, analytical, numerical, experimental.

1. Introduction

During the last years, the utilization of adhesive-bonding techniques have seen a remarkable growth. Besides their lower production cost indeed, these procedures offer several important advantages over conventional mechanical fasteners, such as: high strength-to-weight ratio, resistance to corrosion and degradation in aggressive environments, continuity and impermeability of the joints, efficient bonding of dissimilar or heterogeneous materials and, through a careful selection of the materials, a high capacity for energy and vibration absorption [1].

However, in large assemblies the thickness and shape of the adhesive cord can strongly affect the strength of the joints and thus of the component [2]. This is a well known issue, especially for rigid or toughened structural adhesives, where significant reductions of the maximum load capacity of the joints are observed if the bondline thickness deviates from an optimum value. This phenomenon is sometimes associated to a change in the failure mode (from cohesive to adhesive, generally for thicknesses lower than the optimum one) and in other cases it is produced by a raise in the stress concentration that usually appears in the extremes of the overlaps (when the thickness exceed the optimum one). For a comprehensive overview of these issues the reader is referred to [3, 4] and references therein. For these reasons the compaction process constitutes a critical phase that must be adequately controlled to guarantee the final quality of the joints. In particular, the assembly process must be designed to ensure a final thickness within the admissible ranges, in order to guarantee the required mechanical performance. In certain cases, the adhesive thickness along the bonded areas cannot be controlled through gauges or spacers, thus the final result mainly depends on the forces imposed during compaction.

In this work we analyze these forces by means of analytical tools, a two-phase numerical model and experimental measurements. The test case is the squeeze-flow of an epoxy-based adhesive, whose rheology is modeled according to a viscoplastic constitutive law (Herschel-Bulkley model), fitted with experimental data available from a characterization. An analytical solution is generalized to be valid for any initial shape of the adhesive cord (wedge-shaped in this work). The numerical model is intended as an auxiliary tool, whose utilization in conjunction with the analytical law allows to correctly predict compressive forces in complex adhesive

*Corresponding author
Email address: sizquierdo@ita.es (S. Izquierdo)

Figure 1: (Color online) Experimental system used for the characterization and the squeeze-flow tests.

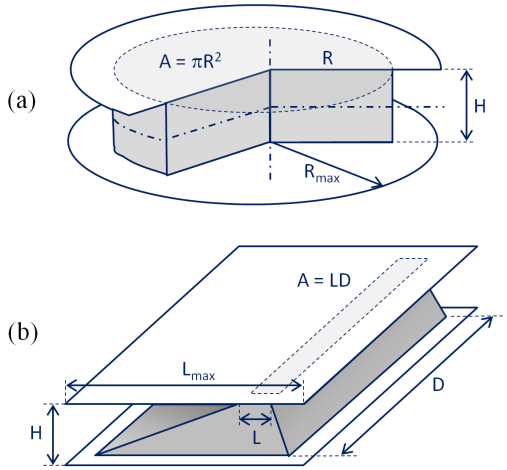

Figure 2: (Color online) Schemes for the analytical solution: cylindrical (a) and wedge-shaped (b) geometries. The dimensions are: H ranges from 10 to 25 mm, L_{max} is 160 mm, R ranges from 15 to 30 mm and D ranges from 100 to 400 mm.

shapes. The aim of this crossed analysis is to provide valuable information about the limits of each technique and about how to combine them to accurately predict compaction forces for different geometries. Finally, the control of the compaction forces allows to optimize the parameter set-up in the assembly process.
The outline of the paper is as follows: the experimental set-up is firstly briefly explained; successively the analytical and numerical approaches are discussed. The results obtained and the comparison between the approaches with experimental data are presented in section 3. A brief discussion of the results and of the proposed methodologies concludes the paper.

2. Methodology

2.1. Experimental set-up

The squeeze tests were performed using the experimental set-up shown in Fig. 1. A squeeze tool, internally designed, was mounted in a MTS Universal Testing Machine (model Alliance RF100) [5]. The tests were conducted with two load cells: a 1 kN load cell for the tests on the cylindrical specimens and a 100 kN one for those on the wedge-shaped specimens. The tests were performed with a crossbeam velocity between 50 mm/min and 250 mm/min. The squeeze tool is based on guided parallel plates. The four vertical columns ensure a uniform distribution of pressure over the specimen. The lower aluminum plate is fixed to the frame plane, whilst the upper one is assembled to the mobile crossbeam of the universal machine. For the squeeze, a wooden block covered by kraftliner paper was mounted on the upper plate using bolts. In order to contain the lateral overflow of the material, for the wedge-shaped specimen additional aluminum profiles were added to the lower plate. The gap between these profiles and the wooden block was adjusted to guarantee a friction-free vertical movement. The adhesive samples were previously prepared on separate plates. The shape of the specimens (cylindrical or wedge-shaped) was obtained by firstly using a palette for a preliminary modeling and then accurately finished with a laser-cut steel. Each specimen was tested on its individual plane used for the preparation, which was correctly positioned and fixed to the universal machine. Force values were instantaneously recorded by TestWorks®4 [6].

2.2. Analytical model

Analytical solutions for squeeze-flow are typically derived for cylindrical samples [7] as shown in Fig. 2 (a). For this case, the following conditions are considered: a constant velocity $V = -dH/dt$; an interplate volume $\pi R_{max}^2 H$, which is assumed to be always full of material and thus the contribution to the force of the overflow (when squeezing beyond R_{max}) is neglected; a rheology given according to the Herschel-Bulkley model, which in scalar form reads:

$$\tau = \tau_0 + K\dot{\gamma}^n; \tag{1}$$

being τ_0 the yield shear-stress threshold, K the consistency index and n the power-law index. This configuration has been previously studied [8, 9], particularly, Adams et al. [10] demonstrated that for no-slip

boundary conditions at the walls and a plasticity number defined as $S = (RVK^{1/n})/(H^2\tau_0^{1/n})$, in the ranges $0 < S < 100$ and $0.1 < n < 1$ the mean pressure has the following form:

$$\overline{p} = \frac{F}{\pi R^2} = \sigma_0 + \frac{R\tau_0}{H}\left[\frac{2}{3} + \frac{2}{n+3}\left(\frac{2n+1}{n}\right)^n S^n\right]; \quad (2)$$

being σ_0 the uniaxial yield stress. It is typically assumed that $R/H >> 1$ and that the contribution of σ_0 is negligible as compared with $R\tau_0/H$. However, these two simplifications must be avoided for generalizing the solution to arbitrary shapes of the sample, see for example Fig. 2 (b). For the generalization, the contact area must be a function of the contact length L. Thus, for cylindrical samples $L = R$ and the contact area is computed as $A = \pi L^2$. For wedge-shaped samples this contact area is $A = LD$. The definition of the generalized plasticity number S is then:

$$S = \frac{LV}{H^2}\left(\frac{K}{\tau_0}\right)^{1/n}; \quad (3)$$

and the generalized expression for the compressive force follows from Eq. (2):

$$F = \sigma_0 A + \frac{2LA}{3H}\tau_0 + \frac{2LAK}{(n+3)H}\left(\frac{2n+1}{n}\right)^n\left(\frac{LV}{H^2}\right)^n + O\left(\frac{H}{L}\right)^2. \quad (4)$$

The yield stress threshold is straightforwardly defined from the above equation in the limit of $V \to 0$ and neglecting σ_0 as:

$$\tau_0 = \frac{3HF}{2LA}. \quad (5)$$

When working at constant force, an expression for the velocity as a function of the force can be obtained from Eq. (4) and can be used to compute the separation height as a function of time as $H(t_n) = H(t_{n-1}) - V\delta t$, where the explicit expression for the squeeze velocity is (neglecting $O(H/L)^2$-terms):

$$V = \frac{H^2}{L}\left(\frac{n}{2n+1}\right)\left[\left(F - A\sigma_0 - \frac{2LA}{3H}\tau_0\right)\frac{(n+3)H}{2LAK}\right]^{1/n}. \quad (6)$$

Making dimensionless the force F with the yield-stress force $(2LA\tau_0)/(3H)$ the dimensionless compressive force F^* is obtained, which is the result of three contributions:

$$F^* = F_s^* + F_n^* + F_h^*. \quad (7)$$

F_s^* is the dimensionless shear force:

$$F_s^* = 1 + \left(\frac{3}{n+3}\right)\left(\frac{2n+1}{n}\right)^n S^n; \quad (8)$$

which dominates at large S (and large L/H). F_n^* is a normal force arising from the uniaxial yield stress σ_0. Considering a Von Mises solid [9], $\sigma_0 = \sqrt{3}\tau_0$ and this force reads:

$$F_n^* = \frac{3\sqrt{3}}{2}\frac{H}{L}; \quad (9)$$

which is typically relevant in a transition region between $S = 1$ and $S \to 0$. The last force F_h^* encompasses all higher order terms, which are mainly related to surface-fluid interactions. These include slip effects, surface tension and any other surface potential related to, for example, electrostatic forces. This forces are expected to be relevant at small S or equivalently at small L/H and/or small shear rates ($\approx V/H$). To approximate the value of this force, we consider that in the regime of $S \to 0$ the flow is at small shear rates and thus in a Newtonian plateau and that there is full slip at the walls. Using this assumptions the following force is obtained [11]:

$$F_h^* = \frac{3}{2}\frac{K}{\tau_0}\left(\frac{H}{L}\right)^2. \quad (10)$$

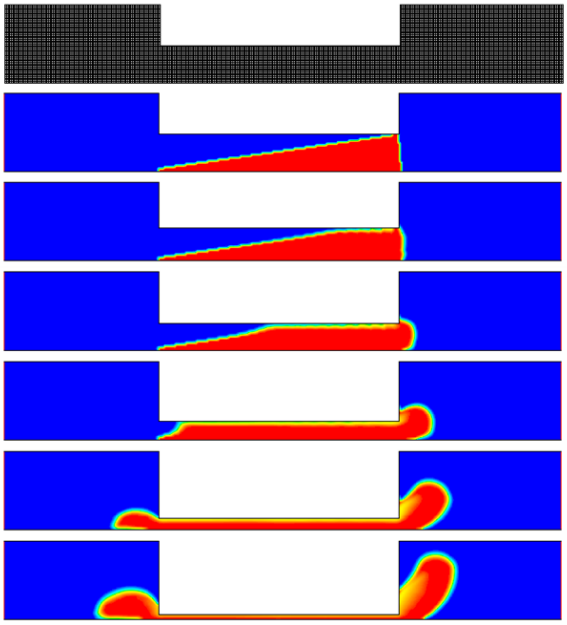

Figure 3: (Color online) Computational mesh and time evolution of the fluid-dynamic solution for $V = 50$ mm/min.

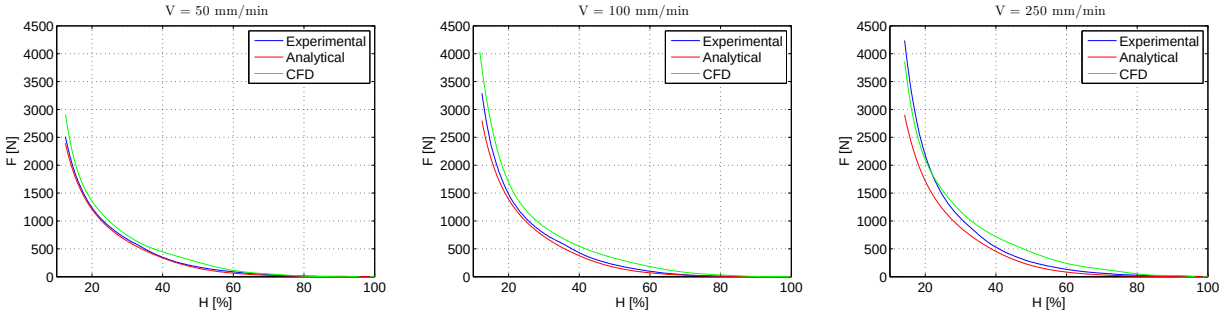

Figure 4: (Color online) Comparison of analytical and numerical solutions with experimental data for the squeeze-flow test at constant velocity. The experimental data and numerical solutions are least-square fitted.

Normal and higher-order forces are usually neglected in squeeze-flow analysis but they are the main forces involved when $L/H >> 1$, which occurs, for example, at the beginning of the compression of a geometry as the one in Fig. 2 (b).
The contact length in arbitrary geometries can be approximated as a weighted function between the initial and the maximum contact length, expressed as a function of the separation height H as:

$$L = \alpha\left(L_{max} - \frac{L_{max}}{H_{max}}H\right) + (1-\alpha)\,L_{max}; \qquad (11)$$

being α a geometric function defined as:

$$\alpha = \frac{1}{1 + exp\left[-\frac{H-\beta}{\gamma}\right]}. \qquad (12)$$

The two fitting coefficients β and γ can be geometrically computed or fitted from CFD and/or experimental data.

2.3. Numerical model

The experimental set-up employed for the characterization of the epoxy-based adhesive is reproduced using the two-dimensional computational domain shown in Fig. (3). The domain consist in a compression chamber, enclosed between two parallel walls. All the boundaries are static, except for the upper central wall, which is used for the compression. The adhesive is modeled as secondary phase and squeezed in the central (thinner) zone of the domain, reproducing a single-lap joint assembly. The multi-phase model adopted is the Volume-Of-Fluid (VOF) method. In this approach a single momentum equation is shared between the phases, therefore the conservation of mass and momentum for the system is given by the incompressible Navier-Stokes equations as:

$$\nabla \cdot \mathbf{v} = 0; \qquad (13)$$

$$\rho\left(\frac{\partial \mathbf{v}}{\partial t} + \mathbf{v}\cdot\nabla\mathbf{v}\right) = -\nabla p + \eta\nabla^2\mathbf{v}; \qquad (14)$$

being ρ the density, p the pressure, $\mathbf{v}$ the velocity and η the dynamic viscosity. The tracking of the interface between the primary (air) and secondary phase (adhesive) is achieved by the solution of a volume fraction equation, which allows Eq. (14) to be shared by the phases through the properties ρ and η. The rheology of the adhesive is given by the Herschel-Bulkley model (Eq. 1), through the viscosity as:

$$\dot{\gamma} < \dot{\gamma}_c : \eta = \frac{2 - \frac{\dot{\gamma}}{\dot{\gamma}_c}}{\dot{\gamma}_c}\tau_0 + K\left[(2-n)(n-1)\frac{\dot{\gamma}}{\dot{\gamma}_c}\right]; \qquad (15)$$

$$\dot{\gamma} > \dot{\gamma}_c : \eta = \frac{\tau_0}{\dot{\gamma}} + K\left(\frac{\dot{\gamma}}{\dot{\gamma}_c}\right)^{n-1}; \qquad (16)$$

being $\dot{\gamma}_c$ a critical shear rate. Equations are solved imposing pressure boundary conditions on the left and right vertical exits, no-slip on the walls. The numerical solution is carried out by finite volume method using the commercial CFD solver ANSYS Fluent® v14.0. We adopt a third order discretization scheme (MUSCL) for momentum and the PRESTO scheme for pressure. The Semi-Implicit Method for Pressure Linked Equations (SIMPLE) is used for the pressure-velocity coupling and the transient scheme is first order implicit.

3. Results

3.1. Adhesive rheology

The analytical solution given by Eq. (4) allows us to use the equipment described in Section 2.1 as a squeeze-

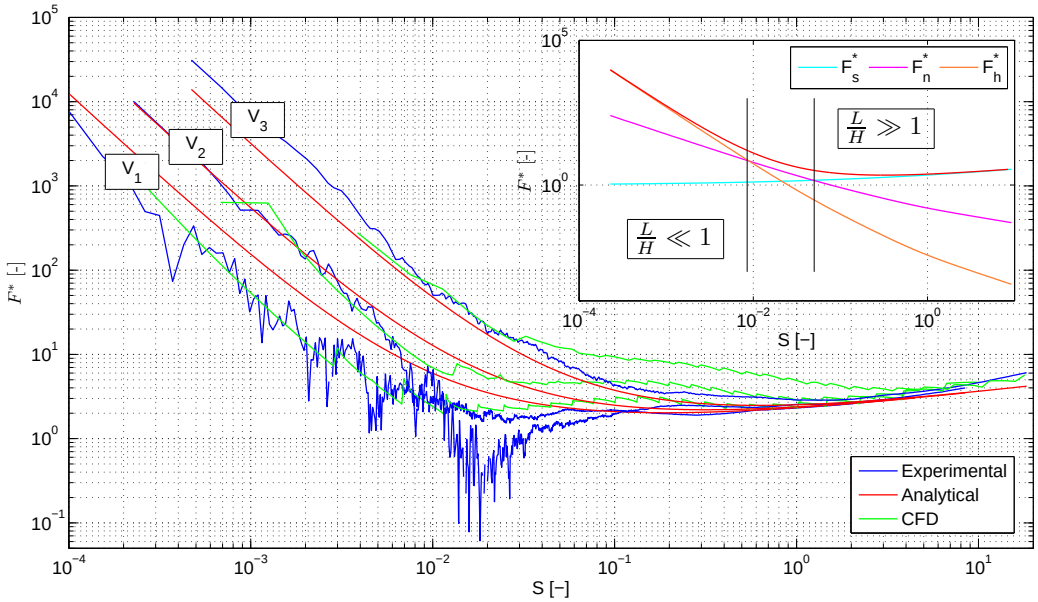

Figure 5: (Color online) Comparison of the dimensionless analytical and numerical solutions with experimental data for $V_1 = 50$ mm/min, $V_2 = 100$ mm/min and $V_3 = 250$ mm/min . Inset: decomposition of the analytical solution F^* for $V_2 = 100$ mm/min (red) in its contributions. For $L/H \gg 1$ the flow regime is shear-dominated, while for $L/H \ll 1$, the flow regime is dominated by $O(L/H)^2$-order forces. In the transition region normal forces prevail.

Table 1: Fitting of the parameters for the Herschel-Bulkley model.

V [m/s]	n [−]	K [$Pa{\cdot}s^n$]
0.05	0.305	232.37
0.05	0.228	251.80
0.10	0.310	230.73
0.10	0.351	219.46
0.25	0.347	325.41
0.25	0.400	284.03
Mean	0.324	257.30

flow rheometer. Thus, the parameters of the Herschel-Bulkley model, n, K and τ_0 in Eq. (1) are obtained by fitting experimental data. For these rheometric experiments, cylindrical test samples of 30 mm radius and 20 mm height are used. The material used is the Spabond 340LV Resin by Gurit [12]. The experiments were carried out in a range of room temperatures between 294 and 296 K. We first performed two creeping experiments at constant force (196 and 412 N) to obtain the yield stress from Eq. (5). The mean value obtained for the yield stress was 372.9 Pa with a standard deviation of 11%. Setting the yield stress to this mean value six experiments at constant velocity were performed (see Table 1) to adjust the values of n and K to experimental data using Eq. (4). The regression coefficients for all cases are $R^2 > 0.99$. The mean values obtained were $n = 0.324$ with a standard deviation of 18% and $K = 257.30$ with a standard deviation of 16%. The use of the squeeze flow rheometer is especially appropriate for the compression of adhesives, as long as the flow has the same shear rate values and history as in the compression of the adhesive in real geometries.

3.2. Adhesive squeeze-flow analysis

Experimental and numerical tests at constant velocity have been conducted and compared to the analytical solution. Dimensional results are reported in Fig. 4. The comparison shows a very good agreement for all cases. The final thickness of the adhesive can be computed by Eq. (5) using the force, the contact area and the yield stress of the adhesive. An additional dimensionless comparison provides insight into the origin of forces during the squeeze-flow process, see Fig. 5. It can be observed that there are three regimes, each one dominated for one of the contributed forces in Eq.

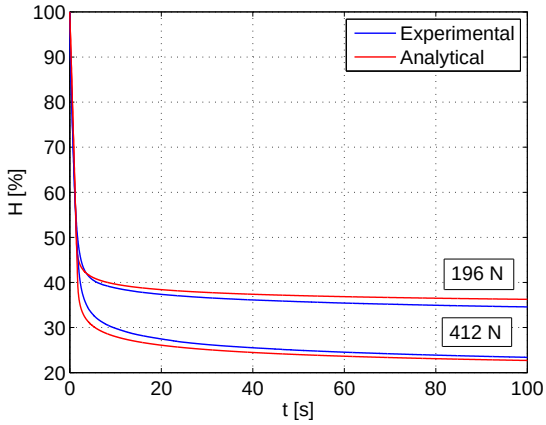

Figure 6: (Color online) Comparison of the analytical solution with experimental data for the squeeze-flow test at constant force.

(7). The $S > 1$ limit is well recovered by the two approaches. In the $S \to 0$ limit both CFD simulations and experimental results show significant oscillations around the expected analytical force. This is due to the nature of forces involved in this regime (i.e. surface tension, wall friction) that are all of the same order and interplay giving a dynamical behavior which has a non-trivial analytical characterization. The real interplaying forces are not exactly the same as in CFD simulations because these latter are also affected by numerical diffusion of the interphase in this stage, but they are anyway of the same order of magnitude. The intermediate regime, in which the normal forces prevail, is not properly recovered by CFD simulations. The reason is that the yield stress is not defined in the same way. In the analytical solution we deal with a Von Mises yield criterion but in the CFD simulation the yield criterion is defined by τ_0 and $\dot{\gamma}_c$. A Von Mises yield criterion or advanced pressure-dependent Drucker-Prager one are not usually implemented in CFD with non-Newtonian rheologies as the conversion from a displacement formulation to a velocity one requires the use of advanced models for the transport of the stress.
Additional tests at constant force were carried out, but only experimental and analytical results are reported in Fig. 6. CFD simulations at constant force for $S < 1$ are difficult to carry out because of the oscillation of forces, as seen in the dimensionless analysis, which makes the simulation unstable.

4. Conclusions

An analytical model for squeeze forces occurring during compaction of bonded joints has been proposed. The analytical solution is generalized to be valid for any initial shape of the adhesive before its squeeze. A two-phase numerical model of the squeeze-flow test has been also introduced. The results obtained with the two approaches showed excellent agreement with experimental data available for a wedge-shaped adhesive geometry. The proposed numerical solution can then be seen as an auxiliary tool to be used in conjunction with the analytical solution for the prediction of forces in complex geometries. The accurate prediction and thus the control of the compressive forces for different shapes of the adhesive cord, allows optimization for example of the position of the jigs (if present) and optimize the amount of material required for the joint execution, reducing the material overflow.
The analysis and decomposition of the analytical solution in its various contributions, provides informations on good-engineering practices to apply when performing CFD simulations of this kind of flows. Particularly, CFD techniques are useful when working at $S > 1$, otherwise forces can be obtained more efficiently from the analytical expression. If simulations for $S < 1$ are needed, it is suggested to elaborate further on surface forces and on yield criteria.
The analytical model developed can be further improved in several ways. For example, in order to take into account the effect of roughness in thin bondlines, the following modeling approaches have been previously adopted [13]: the use of an effective location of straight walls, the use of slip conditions, the use of an effective viscosity or the use of a representative porous-media layer. Another point that could be improved is the use of a temperature-dependent rheology, including the effects of adhesive curing. The latter would be particularly important when analyzing assembling processes with temporal scales in the same range than those of curing.

Acknowledgments

This work has been partially supported by Aeroblade under a private research contract. The authors kindly acknowledge fruitful discussions with P. Muñoz de Felipe, I. Castresana and A. Zabalaandikoetxea during the project.

References

[1] R.D. Adams, J. Comyn, and W.C. Wake. *Structural Adhesive Joints in Engineering*. Springer, 2nd edition, 1997.

[2] L. F. M. Silva, A. Öchsner, and R. D. Adams, editors. *Handbook of Adhesion Technology*. Springer, 2011 edition, 2011.

[3] J.M. Arenas, J.J. Narbón, and C. Alía. Optimum adhesive thickness in structural adhesives joints using statistical techniques based on Weibull distribution. *International Journal of Adhesion and Adhesives*, 30(3):160 – 165, 2010.

[4] P. Davies, L. Sohier, J.-Y. Cognard, A. Bourmaud, D. Choqueuse, E. Rinnert, and R. Créac'hcadec. Influence of adhesive bond line thickness on joint strength. *International Journal of Adhesion and Adhesives*, 29(7):724 – 736, 2009.

[5] MTS Group homepage. URL `http://www.mts.com/en/index.htm`.

[6] MTS TestWorks software. URL `http://www.mts.com/en/products/producttype/test-components/software/testworks/`.

[7] J. Engmann, C. Servais, and A. S. Burbidge. Squeeze flow theory and applications to rheometry: A review. *Journal of Non-Newtonian Fluid Mechanics*, 132(13):1 – 27, 2005.

[8] J.D. Sherwood and D. Durban. Squeeze-flow of a Herschel-Bulkley fluid. *Journal of Non-Newtonian Fluid Mechanics*, 77 (12):115 – 121, 1998.

[9] G. Meeten. Constant-force squeeze flow of soft solids. *Rheologica Acta*, 41(6):557–566, 2002.

[10] M.J. Adams, B. Edmondson, D.G. Caughey, and R. Yahya. An experimental and theoretical study of the squeeze-film deformation and flow of elastoplastic fluids. *Journal of Non-Newtonian Fluid Mechanics*, 51(1):61 – 78, 1994.

[11] J.D. Sherwood and D. Durban. Squeeze flow of a power-law viscoplastic solid. *Journal of Non-Newtonian Fluid Mechanics*, 62(1):35 – 54, 1996.

[12] GURIT Website. URL `http://www.gurit.com/`.

[13] S. Izquierdo, J.R. Valdés, M. Martínez, M. Accolti, S. Woudberg, P. Asinari, M. Miana, and J.P. Du Plessis. Porous-layer model for laminar liquid flow in rough microchannels. *Microfluidics and Nanofluidics*, 9(6):1063–1075, 2010.